Clays Clay Miner., Vol. 70, No. 6:903–915, 2022
https://doi.org/10.1007/s42860-023-00224-w

ORIGINAL PAPER

Calcined Palygorskites as Supplementary Cementitious Materials

Victor Poussardin · Valentin Roux · William Wilson · Michael Paris · Arezki Tagnit-Hamou · Dimitri Deneele

Accepted: 6 March 2023 / Published online: 24 March 2023

Abstract Reducing the environmental footprint of cement is an absolute necessity to meet the commitments of COP26 and to limit global warming to + 1.5°C compared to the pre-industrial level. In this context, particular interest has developed in recent years in the use of calcined clays as supplementary cementitious materials (SCMs). Due to their high reactivity, large reserves and homogeneous distribution on the earth's surface, calcined clays represent a viable alternative to conventional SCMs. Clay minerals are highly variable and numerous, each with their own characteristics. As a result, not all of them have potential for use as SCMs. The present paper investigated the use of palygorskite (a clay that has been relatively poorly studied) as an SCM. Two commercial palygorskites of different grades were selected and their calcination was studied by X-ray diffraction and pozzolanic activity tests. Blended cements incorporating 20% of each calcined palygorskite were prepared and the mechanical performance and resistivity of the mortars measured. The results show that the optimum calcination temperature is 800°C (allowing complete amorphization of the clay fraction and the highest pozzolanic reactivity) for both clays. Mortars made with 80% ordinary Portland cement (OPC) blended with 20% of 800°C calcined palygorskite allowed a significant increase in compressive strength and electrical resistivity compared to the reference (100% OPC). The clay sample with palygorskite as the dominant mineral exhibited the greatest pozzolanic reactivity and mechanical performance in cementitious systems, confirming that palygorskite is a clay mineral with a significant potential for a use as a SCM. The second sample with smaller palygorskite content also allowed a significant increase in mechanical performance. This demonstrated that it is not necessary to use high-purity samples and enhances the value of this type of material.

Keywords Blended cement · Calcined clay · Palygorskite · SCMs

Associate Editor: Andrey G. Kalinichev

V. Poussardin · D. Deneele (✉)
Université Gustave Eiffel, GERS-GIE,
F-44344 Bouguenais, France
e-mail: dimitri.deneele@univ-eiffel.fr

V. Poussardin · V. Roux · M. Paris · D. Deneele
Nantes Université, CNRS, Institut des Matériaux de Nantes Jean Rouxel, IMN, F-44000 Nantes, France

V. Poussardin · V. Roux · W. Wilson · A. Tagnit-Hamou
Université de Sherbrooke, Sherbrooke, QC, Canada

Introduction

Increasing population results in a significant increase in the demand for cement (Cancio Díaz et al., 2017a). Since 1955, cement demand has increased tenfold (Monteiro et al., 2017), resulting in significant CO_2 emissions. Today, the cement industry is estimated

to be responsible for ~8% of global CO_2 emissions (Huntzinger & Eatmon, 2009; Miller et al., 2018), which represents ~2.7 billion tons of CO_2 emitted each year (Bajželj et al., 2013). In this context, the cement industry is working to reduce its carbon footprint by modernizing existing plants to make them more efficient and by developing new technologies (Mari et al., 2021). These include the substitution of fossil fuels in cement kilns by alternative fuels (Rahman et al., 2013), CO_2 capture and storage systems (CCS) (Barker et al., 2009), and the development of alternative low-carbon clinkers (e.g. with large belite content (Staněk & Sulovský, 2015)). These innovations represent a significant cost and/or a long development time (Mari et al., 2021). The reduction of clinker content (by substituting it with other compounds), on the other hand, is a technology that can be implemented today and represents a small cost compared to others (Mari et al., 2021).

In this context, new types of cements incorporating blast furnace slag (Crossin, 2015) or fly ash (Yao et al., 2015) have been developed. Unfortunately, the available quantities of blast furnace slag are not large enough to allow a significant reduction of CO_2 emissions and the energy transition rightly limits the available resources of fly ash from coal combustion (Scrivener et al., 2018). The use of calcined clays as SCMs is attracting increasing interest, in particular, because the available reserves of clays with potential for calcination and use as SCM are large and evenly distributed over the earth's surface (Scrivener et al., 2018). This has led to the development of the Limestone Calcined Clay Cements (LC^3) which are based on the use of metakaolin (Cancio Díaz et al., 2017a; Scrivener et al., 2018). A scientific gap exists in terms of the use of clays other than kaolinite or the other main clays studied such as smectite and illite (Danner et al., 2021; Fernandez et al., 2011).

A previous study that investigated the use of a dolomitic marlstone containing palygorskite (17%) and smectite (16%) as SCM demonstrated the potential of palygorskite (Poussardin et al., 2022). In this context, the aim of the present study was to investigate the use of calcined palygorskite as a new type of SCM by comparing two samples (Plg-1 and Plg-2) containing large amounts of palygorskite. The main objectives were to determine if these palygorskites can be used as SCMs once calcined, and if the percentage of palygorskite in the sample has an influence on the total reactivity. The final objective was to determine the possibility of using so-called low grade Palygorskites as SCMs. This involves a multi-scale study of the calcination, the pozzolanic reactivity, and the mechanical performances in cementitious systems of these two palygorskites.

Materials and Experimental Methods

Materials

The two materials studied (Plg-1 and Plg-2) were commercial palygorskites supplied by an industrial partner. Samples were received in powder form and were analyzed directly. The results of the chemical analysis of the two materials, performed using an Axios Advanced X-ray Fluorescence (XRF) spectrometer by PANalytical (Malvern, UK) are shown in Table 1.

The two materials have an equivalent chemical composition, composed mainly of SiO_2 (54.1 wt.% for Plg-1 and 52.8 wt.% for Plg-2), Al_2O_3 (9.4 wt.% for Plg-1 and 9.8 wt.% for Plg-2), MgO (9.4 wt.% for Plg-1 and 10.5 wt.% for Plg-2), Fe_2O_3 (3.2 wt.% for Plg-1 and 3.3 wt.% for Plg-2), and CaO (2.9 wt.% for Plg-1 and 2.6 wt.% for Plg-2). The quantification of the crystalline phases was carried out using the Rietveld method (see the Supplementary information) on the XRD diffractograms of the raw Plg-1 and Plg-2. Table 2 shows the mineralogical composition of each of these two materials.

Plg-1 and Plg-2 have a relatively similar mineralogy. They are both composed mainly of palygorskite, associated with smectite, quartz, and ankerite. The occurrence of smectite in both materials is explained

Table 1 Chemical analyses of Plg-1 and Plg-2

	Oxides	SiO_2	Al_2O_3	MgO	Fe_2O_3	CaO	P_2O_5	K_2O	TiO_2	LOI (1050°C)
Plg-1	wt.%	54.1	9.4	9.4	3.2	2.9	0.8	0.8	0.4	19.8
Plg-2	wt.%	52.8	9.8	10.5	3.3	2.6	0.9	0.7	0.4	19.5

https://doi.org/10.1007/s42860-023-00224-w Published online by Cambridge University Press

Table 2 Mineralogical composition of Plg-1 and Plg-2

	Phases	Palygorskite	Smectite	Quartz	Ankerite
Plg-1	wt.%	61 (±0.65)	25 (±0.36)	10 (±0.14)	4 (±0.12)
Plg-2	wt.%	73 (±0.70)	21 (±0.44)	4 (±0.15)	2 (±0.1)

by the fact that palygorskite is mainly formed by the alteration of smectite (Krekeler et al., 2005; Xie et al., 2013). It is, therefore, very common to find smectite associated with palygorskite in natural samples.

The particle-size distributions (obtained from powders by laser granulometry using a Mastersizer 2000 laser granulometer by Panalytical, Malvern, UK) of the white, general-use Portland cement (GU-white), the grey, general-use Portland cement (GU-grey), and Plg-1 and Plg-2 (before and after calcination at 800°C) are shown in Tables 3 and 4. The values d10, d50, and d90 indicate the size below which 10%, 50%, or 90% of all particles are found.

X-ray diffraction analysis

X-ray diffraction (XRD) analyses were performed using a PANalytical X'Pert pro MPD diffractometer (Panalytical, Malvern, UK) equipped with a PIXcel 1D detector (active length of 3.347°2θ). The X-ray tube consisted of a copper anode tube (40 kV / 50 mA) that emits CuKα radiation (λ = 1.5418 Å). Measurements were based on a Bragg–Brentano geometry with 0.04 rad Soller slits. Anti-scatter and incident divergence slits were 1/8° and 1/16°, respectively. The diffractograms were acquired between 3 and 70°2θ, with a step size of 0.0131°2θ and a measurement time of 0.75 s per step. The quantification of the crystalline phases of Plg-1 and Plg-2 was carried out using the Rietveld method (see supporting informations) using the Profex/BGMN software (BGMN structure database).

Table 3 Particle-size distributions of the palygorskites (Plg-1 and Plg-2) before and after calcination at 800°C

Label	d10 (μm)	d50 (μm)	d90 (μm)
Plg-1	5	22	67
800°C-Plg-1	4	20	72
Plg-2	4	11	23
800°C-Plg-2	3	9	20

Calcination

The choice of the calcination protocol was made on the basis of the existing literature on the subject (Danner et al., 2018; Garg & Skibsted, 2014, 2016; Krishnan et al., 2019; Trümer et al., 2019). Plg-1 and Plg-2 were calcined using a laboratory furnace in flat alumina crucibles (to ensure a homogeneous calcination) under atmospheric conditions. They were heated from room temperature up to 600, 700, 800, and 900°C with a heating rate of 5°C/min and a residence time at maximum temperature of 1 h. After calcination, the materials were left to cool to room temperature in the oven overnight (with the door closed).

Nuclear magnetic resonance

The ^{27}Al MAS NMR spectra were acquired on a Bruker Avance III 500 MHz spectrometer (Billerica, Massachusetts, USA) using a 2.5 mm MAS probe. The excitation pulse length used was π/13 for a radio frequency field of 11 kHz. The repetition time was 1 s and the MAS frequency was 30 kHz. The ^{29}Si MAS NMR spectra were acquired on a Bruker NEO 300 MHz spectrometer (Billerica, Massachusetts, USA) using a 7 mm MAS probe.

A π/2 excitation pulse length was used, and the MAS frequency was 5 kHz. After several tests of different repetition times, the choice was made to use a time of 10 s in order to ensure quantitative results (except for quartz). However, this has no consequences as quartz is non-reactive. ^{1}H decoupling

Table 4 Particle-size distributions of GU-grey and GU-white

Label	d10 (μm)	d50 (μm)	d90 (μm)
GU-grey	4	21	60
GU-white	2	14	42

https://doi.org/10.1007/s42860-023-00224-w Published online by Cambridge University Press

was performed during all the acquisitions. ^{27}Al spectra were referenced against an aqueous solution of $Al(NO_3)_3$ and ^{29}Si spectra against TMS (tetramethylsilane). The spectral decompositions were done using the *dmfit* software (Massiot et al., 2002).

Pozzolanic activity: isothermal calorimetry

The pozzolanic activity of Plg-1 and Plg-2 calcined at different temperatures was evaluated according to ASTM C1897 (ASTM International, 2020b) by measuring the cumulative heat release. 10 g of dry SCM was mixed with 30 g of calcium hydroxide, 5 g of calcium carbonate, and 54 g of potassium solution (prepared by dissolving 4 g of potassium hydroxide and 20 g of potassium sulfate in 1 L of reagent water) at 1600 r/min for 2 min using a high-shear blender so that a homogeneous paste was achieved. All chemicals were obtained from Thermo Fisher Scientific (Waltham, Massachusetts, USA). Then, 15 g of the paste was cast into calorimeter ampoules and placed in the calorimeter measurement chamber (TAM Air, TA Instruments, Newcastle, Delaware, USA). The cumulative heat release was recorded for 7 days (168 h) after mixing and expressed in J/g of SCM.

Calcined palygorskite-cement blends and compressive strength measurements

Two different blended cements were obtained by mixing 80 wt.% of GU-grey or GU-white with 20 wt.% of 800°C calcined Plg-1 or 800°C calcined Plg-2. All cements were obtained from Cement Roadstone Holdings (CRH, Concord, Ontario, Canada). The objective of blending with GU-grey and GU-white cements was to assess the influence of the addition on the mechanical performance in a conventional system (GU-grey cement), but also to be able to perform solid state NMR measurements in order to evaluate the influence of the Palygorskite on the hydration kinetics (in this case GU-white cement is used to avoid the distortion of the NMR signal induced by iron atoms).

The particle-size distribution of the calcined palygorskites (Table 3) and the two types of cements (Table 4) are of the same order of magnitude, which ensures a homogeneous blend.

The chemical analysis (performed by XRF) of the two cements, GU-grey and GU-white, are reported in Table 5. The main differences were in the proportion of Fe_2O_3, which was very small for GU-white and the proportion of alkali which was greater for GU-grey.

Mortar cubes (50 mm × 50 mm × 50 mm) were then prepared using a constant water:binder ratio of 0.484 and with graded ASTM C109 (ASTM International, 2020a) standard sand (sand:binder = 2.75). Molds were then placed in plastic bags for 20 h until demolding. The demolded mortar cubes were stored in CaO-saturated water until the age of testing. Compressive strength was assessed according to the ASTM C109 loading procedure (ASTM International, 2020a) after 7 and 28 days of hydration. Control mortar cubes were made using 100% GU-grey and 100% GU-white. A polycarboxylate (PC) superplasticizer was used for mortars made with the blended cements to obtain a slump flow equivalent to that of the control mortars.

Electrical resistivity

The electrical bulk resistivity was used to assess the influence of the SCMs on the durability of mortars. The electrical resistivity was evaluated on 50 mm × 50 mm × 50 mm mortar cubes at 28 days of curing. All measurements were made directly after removing the samples from the lime solution and after wiping the surface with a wet towel to remove the excess water. This was done to ensure an equivalent moisture state. Two electrodes were placed on opposite surfaces of the cubes, a voltage was applied, and the potential difference (resistance,

Table 5 Chemical analyses of GU-grey and GU-white

	Oxides	CaO	SiO_2	Al_2O_3	SO_3	MgO	K_2O	TiO_2	Fe_2O_3	Cr_2O_3	SrO	P_2O_5	Na_2O	BaO	LOI
GU-grey	wt.%	61.9	20.7	4.5	3.6	2.1	0.8	0.2	2.5	0	0.1	0.1	0.2	0	2.8
GU-white	wt.%	64.8	21.7	5.1	3.1	0.9	0.2	0.2	0.2	0.2	0	0	0.1	0.1	3.2

https://doi.org/10.1007/s42860-023-00224-w Published online by Cambridge University Press

R) was measured. The electrical resistivity (Ω m) was calculated as $\rho = R.(A/l)$ with R being the electrical resistance (Ω), A the area (m^2) of the cross section of the specimen, and l the length (m) of the specimen.

Results and Discussion

Calcination and reactivity

The XRD analysis (Fig. 1) of the raw Plg-1 and Plg-2 samples revealed the characteristic peaks of palygorskite (Plg), smectite (Sme), quartz (Qz), and ankerite (An). From 600°C, the [001] characteristic peak of the smectite shifted from ~6 to 9°2θ, which is caused by the decrease in the d_{001} value due to the removal of water from the interlayer space (Carniel et al., 2014).

With increasing calcination temperature, the intensity of the characteristic peaks of palygorskite and smectite decreased gradually. They were no longer detectable at 900°C while the characteristics peaks of åkermanite (Ak) and enstatite (En) (Kretz, 1983) appeared. Quartz was not affected by the thermal treatment as its characteristic peaks were still observable after calcination at 900°C. The evolution of the diffractograms of Plg-1 and Plg-2 was similar, and, based on the XRD results, 800°C seems to be the best calcination temperature as it allows an important amorphization of the clay phases while avoiding recrystallization phenomena.

Pozzolanic activity measurements were then carried out at each temperature to determine accurately the optimum calcination temperature of Plg-1 and Plg-2 (Fig. 2). For both Plg-1 and Plg-2, the pozzolanic reactivity increased with the increasing calcination

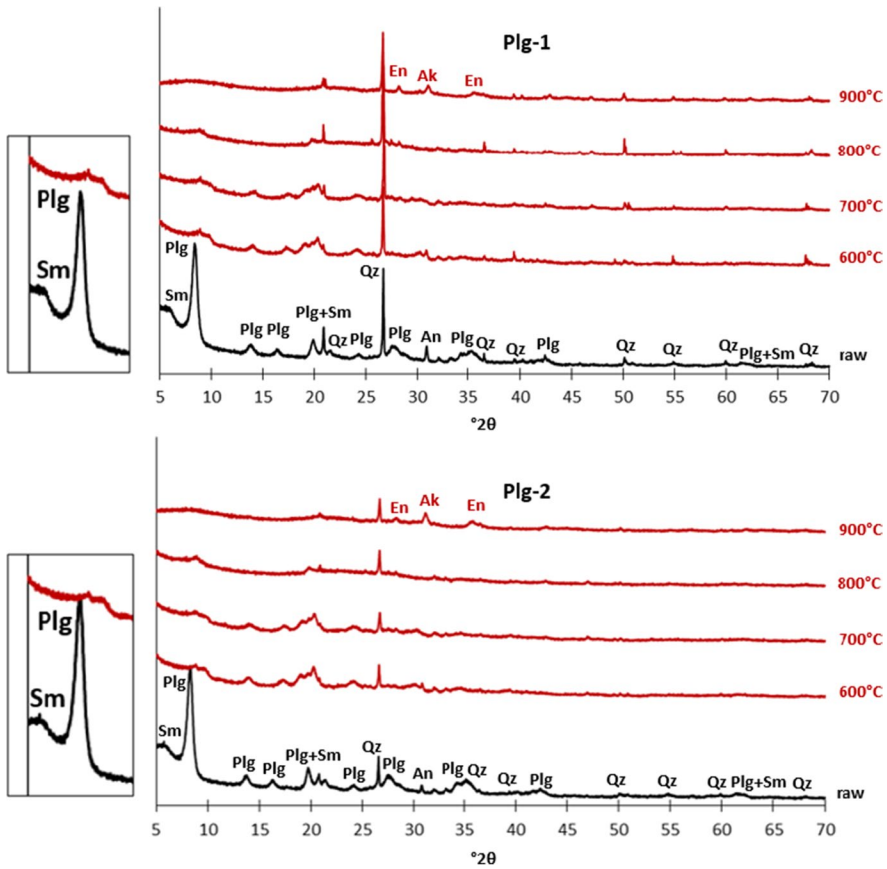

Fig. 1 Evolution of the X-ray diffractograms of Plg-1 and Plg-2 samples as a function of the calcination temperature (with an enlargement of the low-angle area). Plg = palygorskite; Sme = smectite; Qz = quartz; An = ankerite; Ak = akermanite; En = enstatite

https://doi.org/10.1007/s42860-023-00224-w Published online by Cambridge University Press

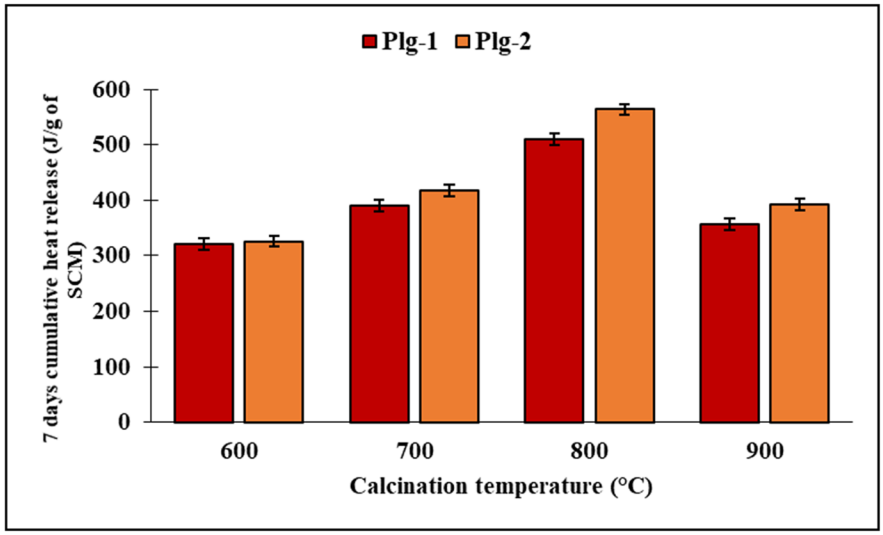

Fig. 2 Evolution of the pozzolanic activity (cumulative heat release) of Plg-1 and Plg-2 samples as a function of the calcination temperature

temperature up to a maximum of 510 J/g of SCM (Plg-1) and 564 J/g of SCM (Plg-2) at 800°C. In a previous study (Poussardin, 2022), a reference palygorskite (containing 79% of palygorskite and 11% of smectite), sample PFl-1 obtained from the Source Clays Repository of The Clay Minerals Society, was tested and demonstrated a pozzolanic activity value of 528 J/g SCM after calcination at 800°C. Plg-1 and Plg-2 (which contain smaller percentages of Palygorskite, 61 and 73%, respectively) exhibited a pozzolanic reactivity equivalent to that of PFl-1 (79% palygorskite).

Ten types of metakaolins varying in purity and other constituent minerals were tested by Londono-Zuluaga et al. (2022) who obtained pozzolanic reactivity values ranging from 250 to 960 J/g of SCM at 7 days. These pozzolanic reactivity values of palygorskite reported here are, therefore, typical for this type of clay and very interesting as they are in the range of metakaolin, which is the current reference for calcined clays.

The pozzolanic reactivity decreased after calcination at 900°C for both Plg-1 and Plg-2 because of the recrystallization phenomena, as highlighted for the XRD analyses. Recrystallization of metastable phases is a well-known phenomenon that leads to a decrease in the total pozzolanic reactivity of the sample (the newly formed phases will not be prone to dissolve and react pozzolanically) (Alujas et al., 2015). Pozzolanic reactivity measurements correlated well with the XRD analysis (Fig. 1); the increase in pozzolanic reactivity followed the loss of crystallinity of the calcined clay phases highlighted by XRD. Plg-1 and Plg-2, despite their difference in mineralogical composition (difference in the total proportion of clay phases as well as the proportion of palygorskite), showed equivalent pozzolanic reactivity at each temperature (the difference between the two was of the same order of magnitude as the measurement uncertainty).

Based on the XRD analysis and the pozzolanic activity test, 800°C is apparently the appropriate calcination temperature for both Plg-1 and Plg-2. This temperature is in agreement with temperatures determined in previous studies on a palygorskite-bearing marlstone (Poussardin et al., 2020) and on a reference palygorskite (Poussardin, 2022). Blended cements incorporating 20 wt.% Plg-1 and Plg-2 calcined at 800°C were then produced to make mortars and measure the compressive strength and resistivity.

Calcined palygorskite-cement systems

Compressive strength on calcined palygorskite grey and white cement mortars

The compressive strength measurements (Fig. 3) were done at 7 and 28 days for mortars M-G-GU

https://doi.org/10.1007/s42860-023-00224-w Published online by Cambridge University Press

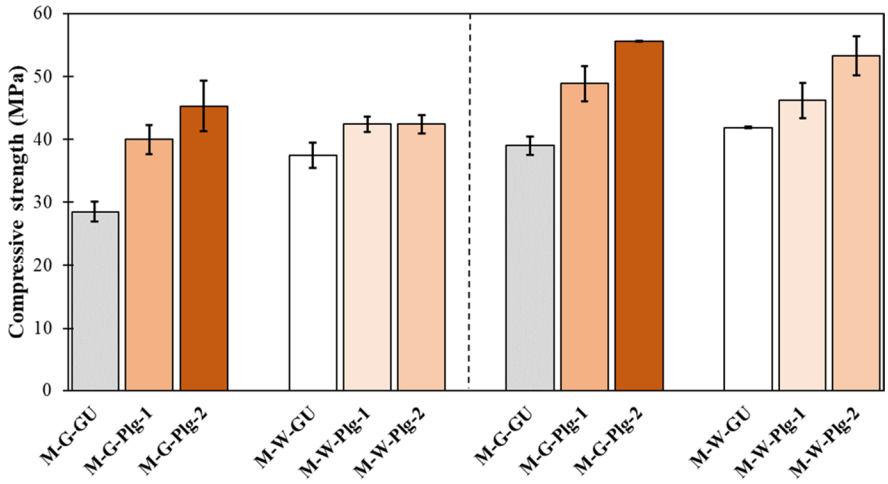

Fig. 3 Compressive strength at 7 (left) and 28 (right) days of M-G-GU, M-G-Plg-1, M-G-Plg-2, M-W-GU, M-W-Plg-1, and M-W-Plg-2

(Mortars-Grey General Use Portland cement), M-G-Plg-1 and M-G-Plg-2 (Mortars-Grey General Use Portland cement incorporating 20 wt.% of Plg-1 and Plg-2 calcined at 800°C, respectively), M-W-GU (white Portland cement), and M-W-Plg-1 and M-W-Plg-2 (white Portland cement incorporating 20 wt.% of Plg-1 and Plg-2 calcined at 800°C, respectively).

After 7 and 28 days of hydration, M-G-Plg-1, M-G-Plg-2, M-W-Plg-1, and M-W-Plg-2 exhibited larger compressive strength values than their respective references (M-G-GU and M-W-GU).

M-G-Plg-2 exhibited compressive strength values equivalent to M-G-Plg-1 at both 7 days (45 and 40 MPa, respectively) and 28 days (56 and 49 MPa, respectively). These results agree with the pozzolanic activity test results which showed an equivalent pozzolanic reactivity of Plg-2 compared to Plg-1 after calcination at 800°C. These results were confirmed in the white Portland cement system as M-W-Plg-2 exhibited equivalent compressive strength values in the M-W-Plg-1 at 7 and 28 days, respectively.

The lower compressive strengths values in the white cement could be explained by the small alkali content (see Table 5) of the white cement in comparison to the grey cement. This will decrease the alkali content in the pore solution and will lead to a decrease in the rate of dissolution of the calcined SCM, thus delaying the pozzolanic reaction (Kawabata & Yamada, 2015).

The partial cement replacement by Plg-1 or Plg-2 calcined at 800°C led to a significant increase in compressive strengths, which confirmed the high pozzolanic reactivity of these two materials. Based on these results, apparently even with a smaller percentage of palygorskite (as for Plg-1), this type of clay showed a significant pozzolanic reactivity.

MAS NMR Analysis

^{29}Si and ^{27}Al MAS NMR analyses were then carried out on pastes of white portland cement blends after 7 and 28 days of hydration to highlight the influence of the SCM on the hydration of white cement.

The evolution of the ^{27}Al MAS NMR spectra obtained for the cement pastes P-W-GU (GU white cement), P-W-Plg-1 (GU white cement blended with 20% of 800°C-Plg-1), and P-W-Plg-2 (GU white cement blended with 20% of 800°C-Plg-2) hydrated for periods of 7 and 28 days are displayed in Fig. 4.

The spectrum of P-GU (at 7 and 28 days) exhibited two main resonances in the spectral region for the 6-fold Al at 13.1 and 9.8 ppm, which can be associated with Al in ettringite (Andersen et al., 2004) and monosulfate (Andersen et al., 2006), respectively. X-ray diffraction analyses were carried out on these hydrated samples and confirmed the presence of ettringite (see the Supporting Information).The shoulder at 4.5 ppm can be associated with sixfold Al from the C-(A)-S–H as described by Kunhi Mohamed et al (2020). The spectrum of P-GU also contained a broad resonance at 70 ppm which corresponds to 4-fold Al

https://doi.org/10.1007/s42860-023-00224-w Published online by Cambridge University Press

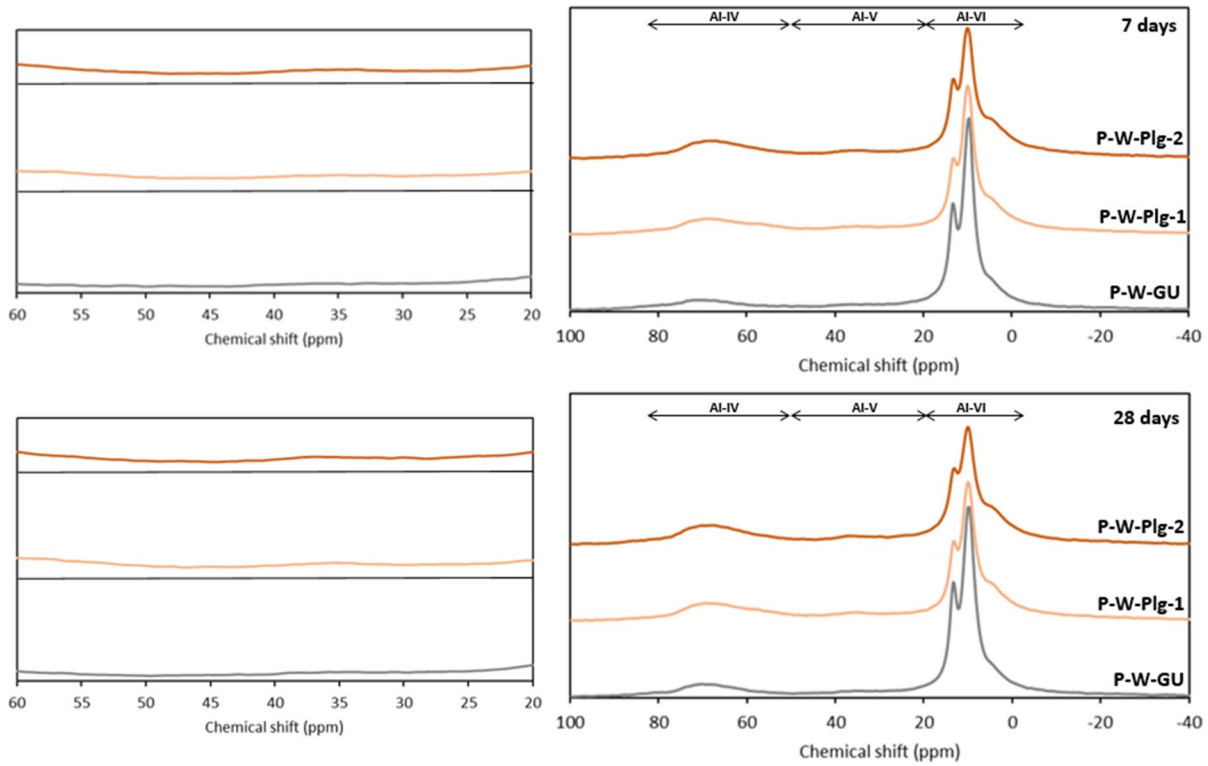

Fig. 4 Evolution of the ^{27}Al MAS NMR spectra (with an enlargement between 60 and 20 ppm) for the cement pastes P-GU, P-W-Plg-1, and P-W-Plg-2 hydrated for 7 and 28 days

and which can be associated with Al incorporated in the C-(A)-S–H chains (Andersen et al., 2003; Richardson et al., 1993).

For the P-W-Plg-1 and P-W-Plg-2 samples, the same characteristic resonances of ettringite (13.1 ppm), monosulfate (9.8 ppm), and Al incorporated in the chains (70 ppm) and interlayers (35 ppm) of C-(A)-S–H were observed. The 35 ppm resonance can also be associated with 5-fold Al from the unreacted calcined clay phases. The addition of Plg-1 and Plg-2 calcined at 800°C did not seem to have much influence on the relative proportions of ettringite and monosulfate (at 7 and 28 days), apart from the dilution effect.The addition of Plg-1 and Plg-2 calcined at 800°C, however, appeared tolead to an increase in the relative proportions of 4- and 5-fold Al, which are associated with Al in the C-(A)-S–H chains and interlayers, respectively. The addition of calcined palygorskite will, therefore, lead to an increase in the incorporation of Al in C-(A)-S–H through pozzolanic reaction. The comparison of P-W-Plg-1 and P-W-Plg-2 indicated that the phenomenon is more pronounced for P-W-Plg-2, which correlates well with the greater pozzolanic reactivity of Plg-2.

The evolution of the ^{29}Si MAS NMR spectra for the cement pastes P-W-GU (GU white cement), P-W-Plg-1 (GU white cement blended with 20% of 800°C-Plg-1), and P-W-Plg-2 (GU white cement blended with 20% of 800°C-Plg-2) hydrated for periods of 7 and 28 days is displayed in Fig. 5.

At 7 days, the spectrum of P-W-GU exhibited a main resonance at -71 ppm, which corresponds to Si atoms in Q^0 configuration (see the Supporting Information) and which can be associated with Si from unhydrated C_2S and C_3S (Cardinaud et al., 2021; Skibsted et al., 1995). The three resonances at -79, -81 and -84 ppm correspond to Si in Q^1, Q^2(1Al), and Q^2 configurations (see the Supporting Information), which can be associated with Si in the C-(A)-S–H (Andersen et al., 2003; Dai et al., 2014; Pardal et al., 2012). Between 7 and 28 days, the relative proportion of Si in Q^0 configuration decreased and

https://doi.org/10.1007/s42860-023-00224-w Published online by Cambridge University Press

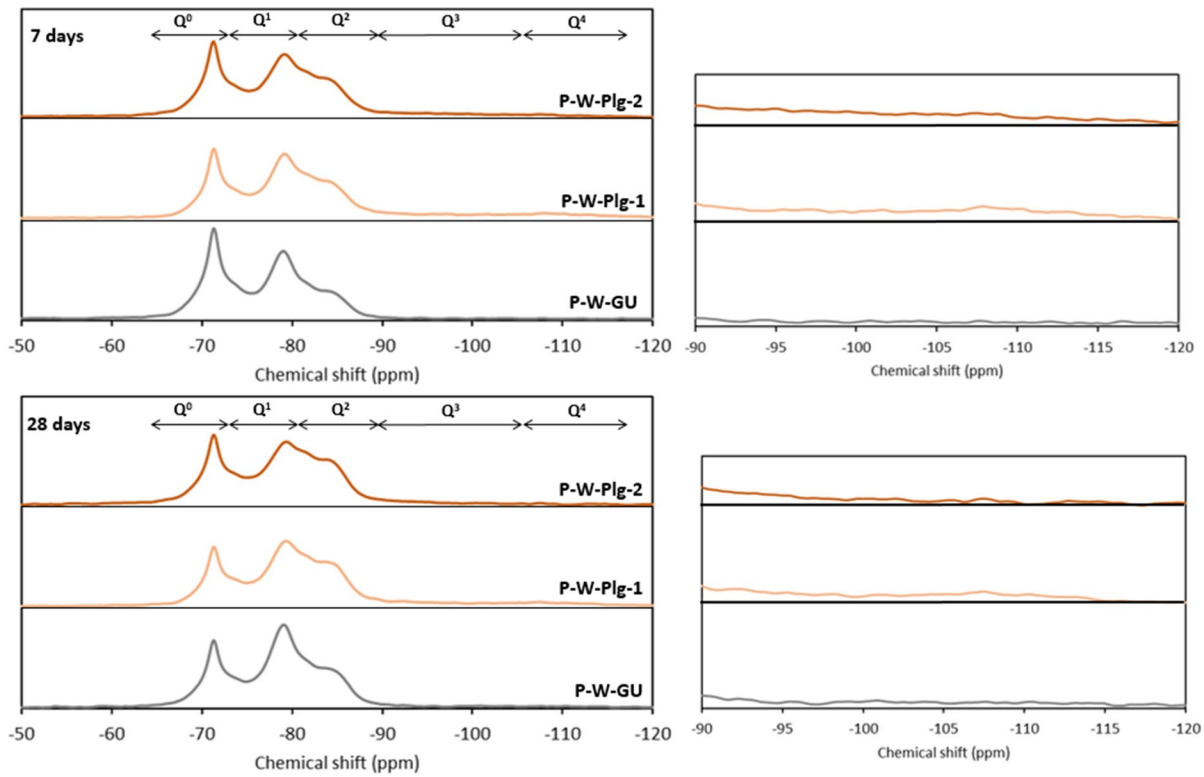

Fig. 5 Evolution of the ^{29}Si MAS NMR spectra (with an enlargement between -90 and -120 ppm) for the cement pastes P-W-GU, P-W-Plg-1, and P-W-Plg-2 hydrated for 7 and 28 days

the relative proportion of Si in Q^1, Q^2(1Al), and Q^2 configurations increased. This reflects a consumption of the C_2S and C_3S associated with the formation of C-(A)-S–H.

At 7 days, the spectra of P-W-Plg-1 and P-W-Plg-2 also exhibited resonances associated with C_2S and C_3S (-71 ppm) as well as with the C-(A)-S–H (Q^1, Q^2(1Al), and Q^2 at -79, -81 and -84 ppm, respectively). The main difference was the presence of a broad resonance in the Q^3 and Q^4 spectral region which can be associated with the Si from the calcined clay phases (palygorskite and smectite) (Poussardin et al., 2022). From 7 to 28 days of hydration, the relative proportion of $C_3S + C_2S$ (Q^0) and calcined clay phases (Q^3 and Q^4) decreased, which is associated with an increase in the relative proportion of C-(A)-S–H (Q^1, Q^2(1Al), and Q^2). These results confirm the pozzolanic reaction of Plg-1 and Plg-2 calcined at 800°C.

To compare accurately the evolution of C-(A)-S–H and calcined clay phases during hydration, a spectral integration quantification was performed. The evolution of the relative proportion of Si from the C-(A)-S–H and from the calcined clay phases as a function of the hydration time for the three systems (P-W-GU, P-W-Plg-1 and P-W-Plg-2) was studied (Fig. 6), not to represent the evolution of the cementitious phases (C_3S, C_2S), but rather to focus on the pozzolanic reactivity only.

For P-W-GU, the relative proportion of C-(A)-S–H increased with the hydration time, which is due to the hydration of the anhydrous phases. For P-W-Plg-1 and P-W-Plg-2, the increase in the relative proportion of C-(A)-S–H correlates with the consumption of the calcined clay phases. After 28 days of hydration, the relative proportion of C-(A)-S–H is greater for P-W-GU- than for P-W-Plg-1 and P-W-Plg-2. The two blends exhibited greater compressive strength values, however. This could be explained by the type of C-(A)-S–H formed in the blends and/or by the filler role of the unreacted calcined clays.

By comparing the two, the consumption of calcined clay phases appeared to be greater for

https://doi.org/10.1007/s42860-023-00224-w Published online by Cambridge University Press

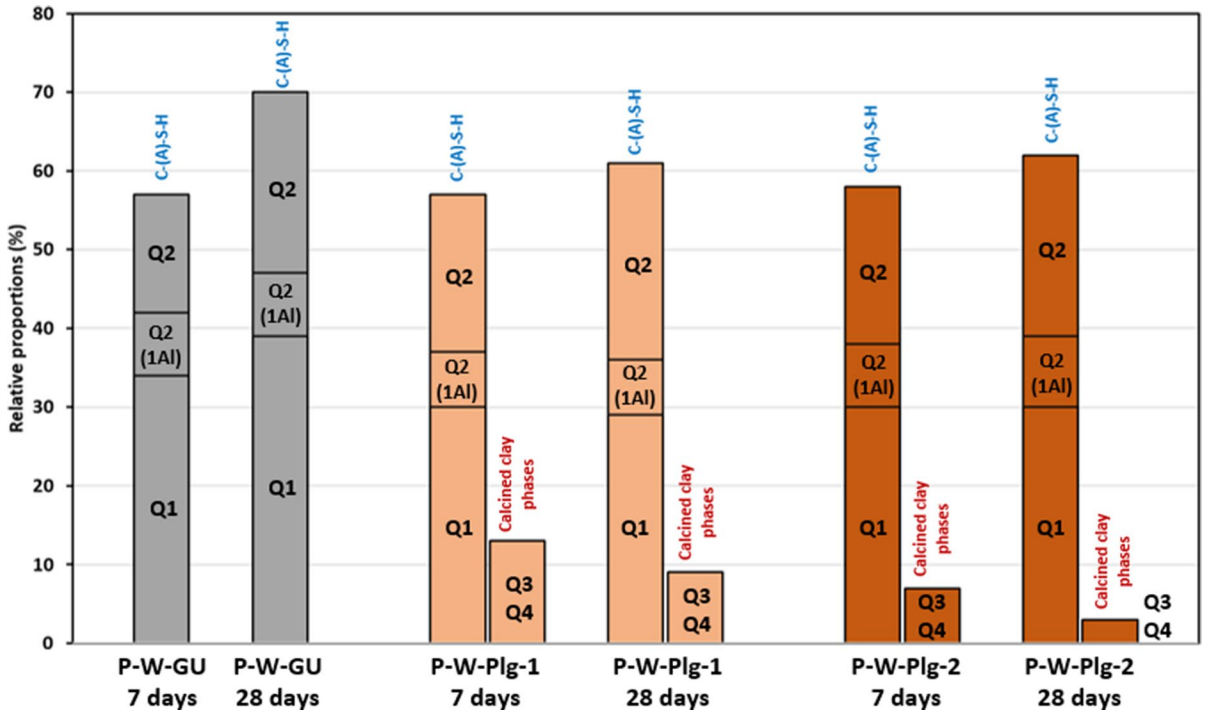

Fig. 6 Evolution of the relative proportions of Si contained in C-(A)-S–H and calcined clay phases of P-W-GU, P-W-Plg-1, and P-W-Plg-2 hydrated for 7 and 28 days

P-W-Plg-2 than for P-W-Plg-1. Despite the greater consumption of calcined clay phases in Plg-2, no particular impact was observed in the relative proportion of C-(A)-S–H compared to Plg-1.

The average chain length of aluminosilicate tetrahedra ($\overline{CL}$) of the C–(A)-S–H structure can be calculated with the following equation using the model of Richardson et al. (1993):

$$\overline{CL} = \frac{2\left[Q^1 + Q^2 + \frac{3}{2}Q^2(1Al)\right]}{Q^1}$$

The average aluminosilicate chain length ($\overline{CL}$) increased with increasing hydration times for P-W-Plg-1 and P-W-Plg-2 (Table 6). The increase in $\overline{CL}$ for the blends P-W-Plg-1 and P-W-Plg-2 by comparison revealed that the increased amount of Al in the hydrating system led to a greater amount of Al incorporated into the C-(A)-S–H structure (Dai et al., 2014). The increase in $\overline{CL}$ correlated well with the ^{27}Al MAS NMR results, which showed an increase in the amount of Al incorporated into the C-(A)-S–H for P-W-Plg-1 and P-W-Plg-2. This increase in $\overline{CL}$ caused by the addition of calcined clay is in agreement with the results of Love et al. (2007). Furthermore, the $\overline{CL}$ values are similar to a system blended with 20% of metakaolin (Dai et al., 2014). However, the increase in $\overline{CL}$ for P-W-Plg-1 and P-W-Plg 2 was not significant enough to explain the differences in compressive strength. The explanation may, therefore, lie more in microstructure and cohesion issues than in C-A-S–H type.

Table 6 Evolution of $\overline{CL}$ of the C-(A)-S–H as function of the hydration time for P-W-GU, P-W-Plg-1, and P-W-Plg-2

	P-W-GU 7 days	P-W-GU 28 days	P-W-Plg-1 7 days	P-W-Plg-1 28 days	P-W-Plg-2 7 days	P-W-Plg-2 28 days
$\overline{CL}$	3,61	3,75	4,09	4,43	4,10	4,47

https://doi.org/10.1007/s42860-023-00224-w Published online by Cambridge University Press

Electrical resistivity on calcined palygorskite grey and white cement mortars

The electrical resistivity at 28 days of the two references (M-G-GU and M-W-GU) and their respective blends (M-G-Plg-1, M-G-Plg-2, M-W-Plg-1 and M-W-Plg-2) is shown in Fig. 7. The electrical resistivity increased significantly in both the grey and white cements when blended with 20 wt.% of 800°C calcined Plg-1 and Plg-2. This gain in electrical resistivity was mainly due to the dilution effect of the clinker with the SCM, which led to a decrease in the total amount of alkalis (Huang & Yan, 2019). Although white cement contains less alkali, the resistivity values appear to be smaller than for grey cement. This can be explained by a more connected porosity, favoring the passage of ions and decreasing the resistivity. In all cases, the addition of 800°C Plg-1 and Plg-2 allowed a significant improvement in the resistivity, suggesting an increased durability for this type of palygorskite blended cement.

Conclusions

A comparative study of the use of two commercial palygorskites (containing different percentages of palygorskite) as SCMs after calcination was carried out. Based on the results, the following conclusions can be drawn:

- A calcination temperature of 800°C is optimal for Plg-1 and Plg-2 and produces the largest pozzolanic reactivity values.
- The preparation of mortars with cements incorporating 20% of Plg-1 and Plg-2 calcined at 800°C showed a significant increase in compressive strength compared to the reference (GU cement-based mortars).
- Plg-1 and Plg-2 have equivalent pozzolanic reactivity, which allows an equivalent compressive strength in the mortars. The difference in the proportion of palygorskite present in each of the samples (61% in Plg-1 and 73% in Plg-2) has no influence on the total pozzolanic reactivity nor on the mechanical performance in the cementitious system.
- In general, palygorskite is a clay mineral with a significant potential for use as a SCM after calcination at 800°C.
- Plg-1, the sample with the smallest proportion of palygorskite exhibited a good pozzolanic activity (heat release of 510 J/g of SCM), yielded a significant increase in mechanical performance compared to the reference. This demonstrates that the use of pure samples is unnecessary and offers new ways of valorization for this type of material.

Further experimentation will continue with the study of samples that contain small proportions of palygorskite (between 20 and 50%) to determine whether a new way of recovery of these so-called low-grade samples is possible.

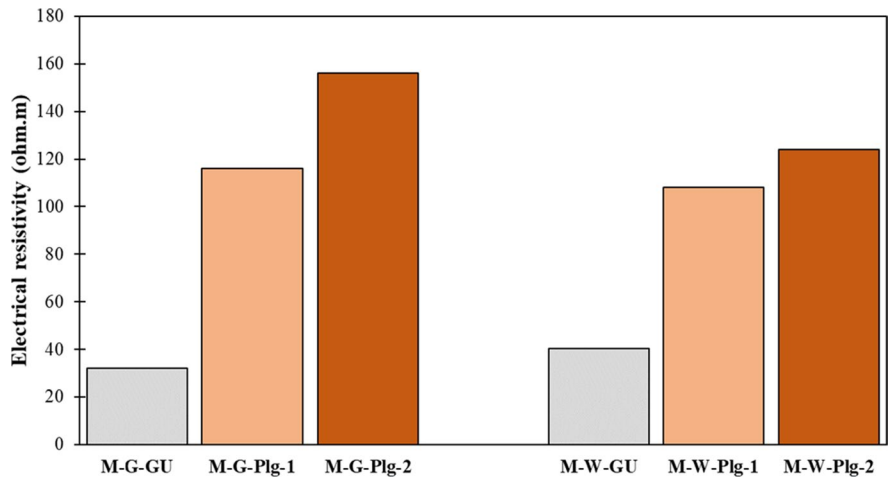

Fig. 7 Electrical resistivity at 28 days of M-G-GU, M-W-GU, M-G-Plg-1, M-G-Plg-2, M-W-Plg-1, and M-W-Plg-2

https://doi.org/10.1007/s42860-023-00224-w Published online by Cambridge University Press

Acknowledgements The authors thank Gustave Eiffel University and Sherbrooke University for funding this research.

Data Availability All data are contained within the article and the supplementary information.

Declarations

Conflict of Interest The authors declare that they have conflict of interest.

References

Alujas, A., Fernández, R., Quintana, R., Scrivener, K. L., & Martirena, F. (2015). Pozzolanic reactivity of low grade kaolinitic clays : Influence of calcination temperature and impact of calcination products on OPC hydration. *Applied Clay Science, 108*, 94–101. https://doi.org/10.1016/j.clay.2015.01.028

Andersen, M. D., Jakobsen, H. J., & Skibsted, J. (2003). Incorporation of Aluminum in the Calcium Silicate Hydrate (C−S−H) of Hydrated Portland Cements : A High-Field ^{27} Al and ^{29} Si MAS NMR Investigation. *Inorganic Chemistry, 42*(7), 2280–2287. https://doi.org/10.1021/ic020607b

Andersen, M. D., Jakobsen, H. J., & Skibsted, J. (2004). Characterization of white Portland cement hydration and the C-S-H structure in the presence of sodium aluminate by 27Al and 29Si MAS NMR spectroscopy. *Cement and Concrete Research, 34*(5), 857–868. https://doi.org/10.1016/j.cemconres.2003.10.009

Andersen, M. D., Jakobsen, H. J., & Skibsted, J. (2006). A new aluminium-hydrate species in hydrated Portland cements characterized by 27Al and 29Si MAS NMR spectroscopy. *Cement and Concrete Research, 36*(1), 3–17. https://doi.org/10.1016/j.cemconres.2005.04.010

ASTM International. (2020a). *ASTM C109M-20, « Standard Test Method for Compressive Strength of Hydraulic Cement Mortars (Using 2-in. Or [50-mm] Cube Specimens) »*. https://doi.org/10.1520/C0109_C0109M-16A

ASTM International. (2020b). *ASTM Standard C1897–20, « Standard Test Methods for Measuring the Reactivity of Supplementary Cementitious Materials by Isothermal Calorimetry and Bound Water Measurements »*. https://doi.org/10.1520/C1897-20

Bajželj, B., Allwood, J. M., & Cullen, J. M. (2013). Designing Climate Change Mitigation Plans That Add Up. *Environmental Science & Technology, 47*(14), 8062–8069. https://doi.org/10.1021/es400399h

Barker, D. J., Turner, S. A., Napier-Moore, P. A., Clark, M., & Davison, J. E. (2009). CO_2 Capture in the Cement Industry. *Energy Procedia, 1*(1), 87–94. https://doi.org/10.1016/j.egypro.2009.01.014

Cancio Díaz, Y., Sánchez Berriel, S., Heierli, U., Favier, A. R., Sánchez Machado, I. R., Scrivener, K. L., Martirena Hernández, J. F., & Habert, G. (2017). Limestone calcined clay cement as a low-carbon solution to meet expanding cement demand in emerging economies. *Development Engineering, 2*, 82–91. https://doi.org/10.1016/j.deveng.2017.06.001

Cardinaud, G., Rozière, E., Martinage, O., Loukili, A., Barnes-Davin, L., Paris, M., & Deneele, D. (2021). Calcined clay – Limestone cements : Hydration processes with high and low-grade kaolinite clays. *Construction and Building Materials, 277*, 122271. https://doi.org/10.1016/j.conbuildmat.2021.122271

Carniel, L. C., Conceição, R. V., Dani, N., Stefani, V. F., Balzaretti, N. M., & dos Reis, R. (2014). Structural changes of potassium-saturated smectite at high pressures and high temperatures : Application for subduction zones. *Applied Clay Science, 102*, 164–171. https://doi.org/10.1016/j.clay.2014.09.037

Crossin, E. (2015). The greenhouse gas implications of using ground granulated blast furnace slag as a cement substitute. *Journal of Cleaner Production, 95*, 101–108. https://doi.org/10.1016/j.jclepro.2015.02.082

Dai, Z., Tran, T. T., & Skibsted, J. (2014). Aluminum Incorporation in the C-S-H Phase of White Portland Cement-Metakaolin Blends Studied by ^{27} Al and ^{29} Si MAS NMR Spectroscopy. *Journal of the American Ceramic Society, 97*(8), 2662–2671. https://doi.org/10.1111/jace.13006

Danner, T., Norden, G., & Justnes, H. (2018). Characterisation of calcined raw clays suitable as supplementary cementitious materials. *Applied Clay Science, 162*, 391–402. https://doi.org/10.1016/j.clay.2018.06.030

Danner, T., Norden, G., & Justnes, H. (2021). Calcareous smectite clay as a pozzolanic alternative to kaolin. *European Journal of Environmental and Civil Engineering, 25*(9), 1647–1664. https://doi.org/10.1080/19648189.2019.1590741

Fernandez, R., Martirena, F., & Scrivener, K. L. (2011). The origin of the pozzolanic activity of calcined clay minerals : A comparison between kaolinite, illite and montmorillonite. *Cement and Concrete Research, 41*(1), 113–122. https://doi.org/10.1016/j.cemconres.2010.09.013

Garg, N., & Skibsted, J. (2014). Thermal Activation of a Pure Montmorillonite Clay and Its Reactivity in Cementitious Systems. *The Journal of Physical Chemistry C, 118*(21), 11464–11477. https://doi.org/10.1021/jp502529d

Garg, N., & Skibsted, J. (2016). Pozzolanic reactivity of a calcined interstratified illite/smectite (70/30) clay. *Cement and Concrete Research, 79*, 101–111. https://doi.org/10.1016/j.cemconres.2015.08.006

Huang, L., & Yan, P. (2019). Effect of alkali content in cement on its hydration kinetics and mechanical properties. *Construction and Building Materials, 228*, 116833. https://doi.org/10.1016/j.conbuildmat.2019.116833

Huntzinger, D. N., & Eatmon, T. D. (2009). A life-cycle assessment of Portland cement manufacturing: Comparing the traditional process with alternative technologies. *Journal of Cleaner Production, 17*(7), 668–675. https://doi.org/10.1016/j.jclepro.2008.04.007

Kawabata, Y., & Yamada, K. (2015). Evaluation of Alkalinity of Pore Solution Based on the Phase Composition of Cement Hydrates with Supplementary Cementitious Materials and its Relation to Suppressing ASR Expansion. *Journal of Advanced Concrete Technology, 13*(11), 538–553. https://doi.org/10.3151/jact.13.538

Krekeler, M. P. S., Hammerly, E., Rakovan, J., & Guggenheim, S. (2005). Microscopy Studies of the Palygorskite-to-Smectite Transformation. *Clays and Clay Minerals, 53*(1), 92–99. https://doi.org/10.1346/CCMN.2005.0530109

Kretz, R. (1983). Symbols for rock-forming minerals. *American Mineralogist, 68*, 277–279.

Krishnan, S., Emmanuel, A. C., Shah, V., Parashar, A., Mishra, G., Maity, S., & Bishnoi, S. (2019). Industrial production of limestone calcined clay cement : Experience and insights. *Green Materials, 7*(1), 15–27. https://doi.org/10.1680/jgrma.18.00003

Kunhi Mohamed, A., Moutzouri, P., Berruyer, P., Walder, B., Siramanont, J., Harris, M., Negroni, M., Galmarini, S., Parker, S., Scrivener, K., Emsley, L., & Bowen, P. (2020). The Atomic-Level Structure of Cementitious Calcium Aluminate Silicate Hydrate. *Journal of American Ceramic Society, 142*(25), 11060–11071. https://doi.org/10.1021/jacs.0c02988

Londono-Zuluaga, D., Gholizadeh-Vayghan, A., Winnefeld, F., Avet, F., Ben Haha, M., Bernal, S. A., Cizer, Ö., Cyr, M., Dolenec, S., Durdzinski, P., Haufe, J., Hooton, D., Kamali-Bernard, S., Li, X., Marsh, A. T. M., Marroccoli, M., Mrak, M., Muy, Y., Patapy, C., … Scrivener, K. L. (2022). Report of RILEM TC 267-TRM phase 3 : Validation of the R3 reactivity test across a wide range of materials. *Materials and Structures*, *55*(5), 142. https://doi.org/10.1617/s11527-022-01947-3

Love, C. A., Richardson, I. G., & Brough, A. R. (2007). Composition and structure of C-S–H in white Portland cement–20% metakaolin pastes hydrated at 25°C. *Cement and Concrete Research, 37*(2), 109–117. https://doi.org/10.1016/j.cemconres.2006.11.012

Mari, E., Sourisseau, S., Bouxin, A., Borde, C., Padilla, S., & Gourdon, T. (2021). *ADEME : Plan de Transition Sectoriel de l'industrie cimentière en France : Rapport final. 187 pages.*

Massiot, D., Fayon, F., Capron, M., King, I., Le Calvé, S., Alonso, B., Durand, J.-O., Bujoli, B., Gan, Z., & Hoatson, G. (2002). Modelling one- and two-dimensional solid-state NMR spectra : Modelling 1D and 2D solid-state NMR spectra. *Magnetic Resonance in Chemistry, 40*(1), 70–76. https://doi.org/10.1002/mrc.984

Miller, S. A., John, V. M., Pacca, S. A., & Horvath, A. (2018). Carbon dioxide reduction potential in the global cement industry by 2050. *Cement and Concrete Research, 114*, 115–124. https://doi.org/10.1016/j.cemconres.2017.08.026

Monteiro, P. J. M., Miller, S. A., & Horvath, A. (2017). Towards sustainable concrete. *Nature Materials, 16*(7), 7. https://doi.org/10.1038/nmat4930

Pardal, X., Brunet, F., Charpentier, T., Pochard, I., & Nonat, A. (2012). 27 Al and 29Si Solid-State NMR Characterization of Calcium-Aluminosilicate-Hydrate. *Inorganic Chemistry, 51*(3), 3. https://doi.org/10.1021/ic202124x

Poussardin, V. (2022). La Palygorskite calcinée comme ajout cimentaire : Une étude comparative avec le métakaolin. *Academic Journal of Civil Engineering, 40*(1), 1. https://doi.org/10.26168/ajce.40.1.87

Poussardin, V., Paris, M., Tagnit-Hamou, A., & Deneele, D. (2020). Potential for calcination of a palygorskite-bearing argillaceous carbonate. *Applied Clay Science, 198*, 105846. https://doi.org/10.1016/j.clay.2020.105846

Poussardin, V., Paris, M., Wilson, W., Tagnit-Hamou, A., & Deneele, D. (2022). Calcined palygorskite and smectite bearing marlstones as supplementary cementitious materials. *Materials and Structures, 55*(8), 224. https://doi.org/10.1617/s11527-022-02053-0

Rahman, A., Rasul, M. G., Khan, M. M. K., & Sharma, S. (2013). Impact of Alternative Fuels on the Cement Manufacturing Plant Performance : An Overview. *Procedia Engineering, 56*, 393–400. https://doi.org/10.1016/j.proeng.2013.03.138

Richardson, I. G., & Groves, G. W. (1993). The incorporation of minor and trace elements into calcium silicate hydrate (C-S-H) gel in hardened cement pastes. *Cement and Concrete Research, 23*(1), 1. https://doi.org/10.1016/0008-8846(93)90143-W

Richardson, I. G., Brough, A. R., Brydson, R., Groves, G. W., & Dobson, C. M. (1993). Location of Aluminum in Substituted Calcium Silicate Hydrate (C-S-H) Gels as Determined by 29Si and 27Al NMR and EELS. *Journal of the American Ceramic Society, 76*(9), 2285–2288. https://doi.org/10.1111/j.1151-2916.1993.tb07765.x

Scrivener, K., Martirena, F., Bishnoi, S., & Maity, S. (2018). Calcined clay limestone cements (LC3). *Cement and Concrete Research*, *114*. https://doi.org/10.1016/j.cemconres.2017.08.017

Skibsted, J., Jakobsen, H. J., & Hall, C. (1995). Quantification of calcium silicate phases in Portland cements by 29Si MAS NMR spectroscopy. *Journal of the Chemical Society, Faraday Transactions, 91*(24), 4423. https://doi.org/10.1039/ft9959104423

Staněk, T., & Sulovský, P. (2015). Active low-energy belite cement. *Cement and Concrete Research, 68*, 203–210. https://doi.org/10.1016/j.cemconres.2014.11.004

Trümer, A., Ludwig, H.-M., Schellhorn, M., & Diedel, R. (2019). Effect of a calcined Westerwald bentonite as supplementary cementitious material on the long-term performance of concrete. *Applied Clay Science, 168*, 36–42. https://doi.org/10.1016/j.clay.2018.10.015

Xie, Q., Chen, T., Zhou, H., Xu, X., Xu, H., Ji, J., Lu, H., & Balsam, W. (2013). Mechanism of palygorskite formation in the Red Clay Formation on the Chinese Loess Plateau, northwest China. *Geoderma, 192*, 39–49. https://doi.org/10.1016/j.geoderma.2012.07.021

Yao, Z. T., Ji, X. S., Sarker, P. K., Tang, J. H., Ge, L. Q., Xia, M. S., & Xi, Y. Q. (2015). A comprehensive review on the applications of coal fly ash. *Earth-Science Reviews, 141*, 105–121. https://doi.org/10.1016/j.earscirev.2014.11.016